Submitted 2015 October 7; accepted 2016 May 25
Preprint typeset using LaTeX style emulateapj v. 5/2/11

arXiv:1511.00392v2 [astro-ph.CO] 25 May 2016

A DETECTION OF BARYON ACOUSTIC OSCILLATIONS FROM THE DISTRIBUTION OF GALAXY CLUSTERS

Tao Hong, J. L. Han, and Z. L. Wen
National Astronomical Observatories, Chinese Academy of Sciences, 20A Datun Road, Chaoyang District, Beijing 100012, China.
bartonhongtao@gmail.com, hjl@nao.cas.cn

Submitted 2015 October 7; accepted 2016 May 25

ABSTRACT

We calculate the correlation function of 79,091 galaxy clusters in the redshift region of $z \leq 0.5$ selected from the WH15 cluster catalog. With a weight of cluster mass, a significant baryon acoustic oscillation (BAO) peak is detected on the correlation function with a significance of 3.7σ. By fitting the correlation function with a ΛCDM model curve, we find $D_v(z=0.331)r_d^{fid}/r_d = 1261.5 \pm 48$ Mpc which is consistent with the Planck 2015 cosmology. We find that the correlation function of the higher mass sub-sample shows a higher amplitude at small scales of $r < 80\ h^{-1}$Mpc, which is consistent with our previous result. The 2D correlation function of this large sample of galaxy clusters shows a faint BAO ring with a significance of 1.8σ, from which we find that the distance scale parameters on directions across and along the line-of-sight are $\alpha_\sigma = 1.02 \pm 0.06$ and $\alpha_\pi = 0.94 \pm 0.10$, respectively.

Subject headings: cosmology: observations — galaxies: clusters: general — large-scale structure of universe

1. INTRODUCTION

The matter distribution in the Universe is homogeneous and isotropic on large scales. However, large-scale structures start to emerge from the matter distribution on smaller scales ($\lesssim 100\ h^{-1}$Mpc, Geller & Huchra 1989; Gott et al. 2005; Scrimgeour et al. 2012). The Baryon Acoustic Oscillations (BAO) are an imprint of the oscillations in the early Universe when baryons and photons were tightly coupled (Peebles & Yu 1970; Sunyaev & Zeldovich 1970). The scale of the BAO can be used as a 'standard ruler' to measure cosmological distances. For example, the reduced distance $D_v(z)$ was firstly introduced by Eisenstein et al. (2005):

$$D_v(z) = \left[(1+z)^2 D_A(z)^2 \frac{cz}{H(z)}\right]^{1/3}, \quad (1)$$

where $H(z)$ is the Hubble parameter and $D_A(z)$ is the comoving angular diameter distance. The measurement of the BAO signals provide a powerful tool to constrain the cosmology parameters which determine $D_v(z)$.

The BAO signal was firstly detected by Eisenstein et al. (2005) and Cole et al. (2005) using galaxy redshift data from the Sloan Digital Sky Survey (SDSS, York et al. 2000) and the 2dF Galaxy Redshift Survey (2dFGRS, Colless et al. 2001). After that, similar measurements of the BAO were confirmed by later SDSS data releases (Tegmark et al. 2006; Percival et al. 2007; Kazin et al. 2010; Anderson et al. 2012, 2014) and other galaxy surveys (Blake et al. 2011; Beutler et al. 2011). In addition to galaxies, the Lyα forests were used as a tracer to search the BAO signal at higher redshifts. For example, the BAO feature was detected clearly by using SDSS Lyα forest samples at redshift $z \sim 2.3$ (Busca et al. 2013; Delubac et al. 2015).

Galaxy clusters are the largest gravitationally bound systems in the Universe, trace the higher density peaks in the matter distribution field than galaxies, which makes them a great probe for BAO detection. By calculating the 2-point correlation function and power spectrum of maxBCG clusters (Koester et al. 2007a,b), Estrada et al. (2009) and Hütsi (2010) reported weak detections of BAO signature. Hong et al. (2012) extracted a spectroscopic sample of 13,904 clusters from Wen et al. (2009) in the redshift region of $z \leq 0.4$, and detected the BAO signature from the cluster correlation function with a significance of $\sim 1.9\sigma$. Veropalumbo et al. (2014) further improved this result with a significance of $\sim 2.5\sigma$ by using an updated cluster catalog of Wen et al. (2012).

In this paper, we calculate and analyze the correlation function of 79,091 clusters from Wen & Han (2015, WH15 hereafter) with the spectroscopic redshift information updated to SDSS Data Release 12 (SDSS DR12, Alam et al. 2015). The cluster sample is described in Section 2. The method to calculate the two-point correlation function and the theoretical model to analyze the function are introduced in Section 3, and we present the correlation function results for the whole sample and 6 sub-samples in subsections. The 2D correlation function of this currently largest sample of galaxy clusters are presented and discussed in Section 4. Conclusions are given in Section 5.

Throughout this paper, we adopt a flat ΛCDM cosmology following Planck 2015 results (Planck Collaboration et al. 2015), with $h = 0.68$, $\Omega_m = 0.31$, $\Omega_\Lambda = 0.69$, $\sigma_8 = 0.81$, where $h \equiv H_0/100$ kms^{-1}Mpc^{-1}.

2. DATA

Using the photometric data from SDSS-III, Wen et al. (2012) identified 132,684 galaxy clusters with a redshift range of $z < 0.8$. All these clusters have a richness of $R_{L*} \geq 12$ and more than 8 member galaxies within r_{200}. Monte Carlo simulations give a false detection rate of less than 6% for the whole catalog. The completeness is more than 95% in the redshift range of $z < 0.42$ for massive clusters with $M_{200} > 1 \times 10^{14}M_\odot$. By applying a new richness estimation together with the latest SDSS

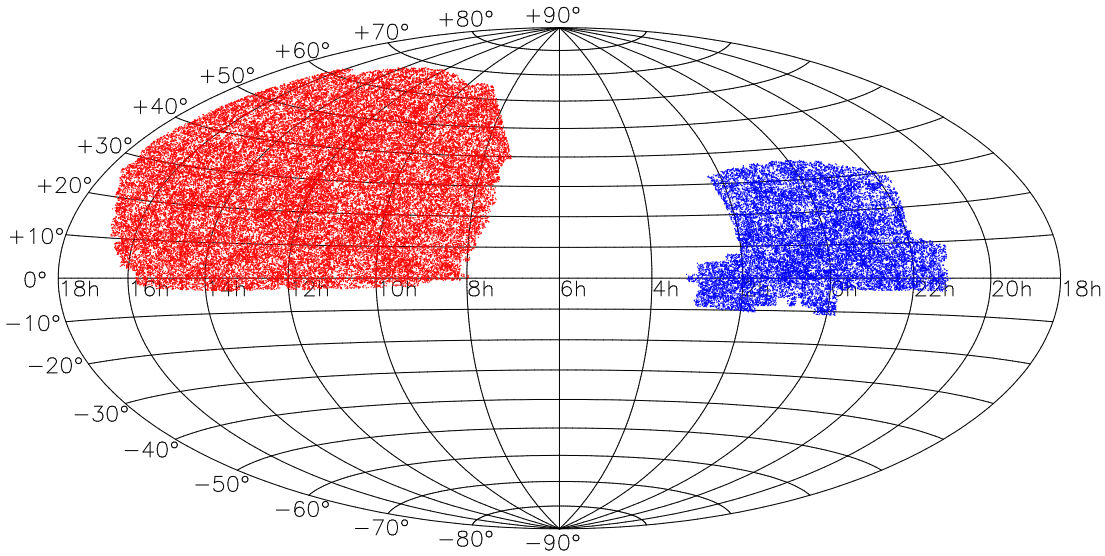

FIG. 1.— Sky distribution of 79,091 clusters in our sample, with an Aitoff projection centered at (RA, DEC) = $(6h, 0°)$. There are 57,647 clusters in the Northern Galactic Cap and 21,444 clusters in the Southern Galactic Cap.

DR12 spectroscopic data (Alam et al. 2015), WH15 detected 25,000 high redshift clusters which helps to get a high completeness in the region of $z < 0.6$ for clusters of $M_{500} > 1 \times 10^{14}\mathrm{M}_{\odot}$.

Although the photometric redshift is good enough for identifying the galaxy clusters, its large uncertainties will affect correlation function calculations and hence obstruct the detection of BAO signature (Blake & Bridle 2005; Zhan et al. 2008). For this work, we use a sample of 79,091 clusters derived from the WH15 cluster catalog, which have a spectroscopic redshift from SDSS DR12 data (Alam et al. 2015), including 57,647 clusters from the Northern Galactic Cap and 21,444 clusters from the Southern Galactic Cap, as shown in Figure 1. The whole sample covers a sky region of $\sim 11,000$ square degree in total. To make sure our sample has a high completeness, we only use the spectroscopic clusters within the redshift range of $z \leq 0.5$ with a mean redshift $\overline{z} = 0.331$ (see Figure 2).

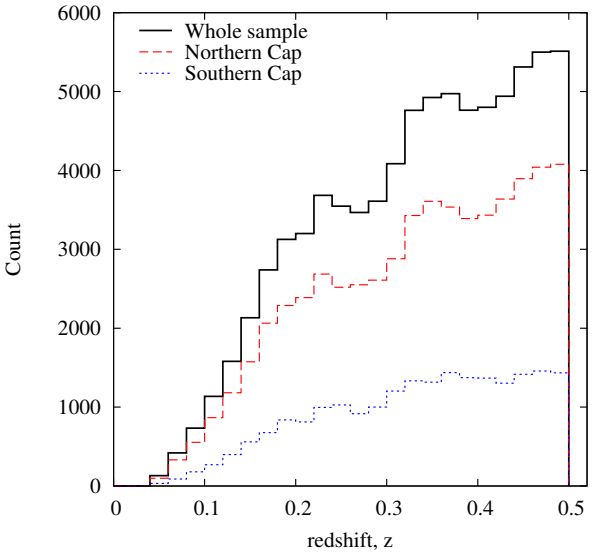

FIG. 2.— Redshift distribution of 79,091 clusters in our sample as indicated by black solid line. The dashed line and dotted line indicate the distributions of clusters in the Northern Cap and Southern Cap, respectively.

3. THE TWO-POINT CORRELATION FUNCTIONS

We calculate the 2-point correlation function $\xi(r)$ of cluster samples using the Landy-Szalay estimator (Landy & Szalay 1993):

$$\xi(r) = \left[DD(r)\frac{N_{RR}}{N_{DD}} - 2\,DR(r)\frac{N_{RR}}{N_{DR}} + RR(r) \right] / RR(r), \quad (2)$$

where $DD(r)$, $DR(r)$ and $RR(r)$ stand for the weighted number of data-data pairs, data-random pairs and random-random pairs within a separation annulus of $r \pm \Delta r/2$, respectively. N_{DD}, N_{DR} and N_{RR} are the weighted normalization factors. The random sample used here is 16 times larger than the data sample, which minimizes the shot noise effect during the calculations. The random sample shares the same sky area and the same redshift distribution as the real cluster sample.

More massive galaxy clusters trace more massive dark matter halos, which should reflect large-scale structures with a larger weight. To reveal the BAO feature from the complex matter distribution background, the more massive clusters should have higher weights than low mass ones. The galaxy clusters in this sample have a mass in the range from $10^{13.5}\mathrm{M}_{\odot}$ to $10^{15}\mathrm{M}_{\odot}$ as shown in Figure 3. Wen & Han (2015) have related the cluster mass with the r-band optical luminosity or the richness in their paper. Here, we adopt a linear weight for cluster mass as

$$w_{\mathrm{mass}} = M_{500}/10^{14}\mathrm{M}_{\odot}, \quad (3)$$

where M_{500} is the cluster mass within the radius where the mean density is 500 times of the critical density of the Universe (see WH15 for more details).

The completeness of clusters in the sample depends on the mass of cluster. The completeness can reach 100% in the high mass end of the sample distribution, but only about 50% in the low mass end. To correct the effect of the detection rate, we apply a weight of $w_{\mathrm{completeness}}$ as the reciprocal of the mass-dependent detection rate

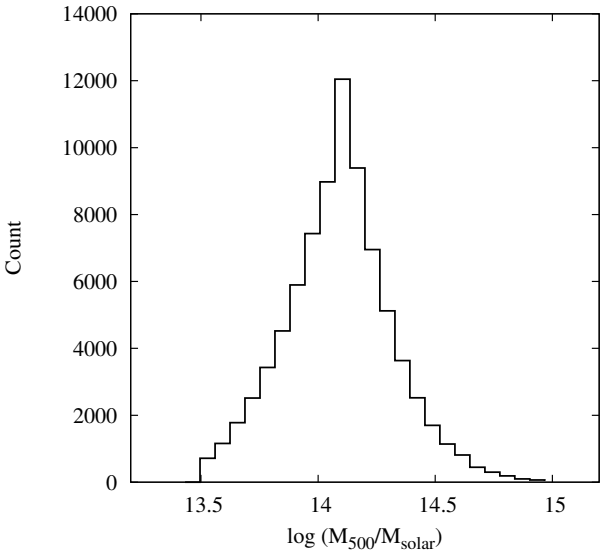

FIG. 3.— Mass distribution of clusters in our cluster sample.

provided in the Figure 6 of Wen et al. (2012). The total weight of the i^{th} cluster for the 2-point correlation function is thus taken as the combination of the above two weights:

$$w_i = w_{\rm mass} \times w_{\rm completeness}. \quad (4)$$

The error covariance of the correlation function is estimated by using the log-normal mock catalogs. The log-normal error estimation method was introduced by Coles & Jones (1991), and adopted by several BAO analysis works (e.g. Beutler et al. 2011; Blake et al. 2011). We create the log-normal realizations using a model power spectrum:

$$P(k) = b^2(1 + \frac{2}{3}\beta + \frac{1}{5}\beta^2)P_{lin}(\overline{z}, k), \quad (5)$$

where b is the bias measured by fitting the cluster correlation function using the model curve with the covariance matrix estimated by the jackknife method, $\beta = \Omega_m^{0.55}/b$, $P_{lin}(\overline{z}, k)$ is the linear power spectrum obtained from the CAMB package (Lewis et al. 2000) at the mean redshift $\overline{z} = 0.331$. In total, 100 log-normal mock catalogs are generated in the boxes of $3000 \times 3000 \times 3000$ h^{-1}Mpc with $600 \times 600 \times 600$ cells. The large box size makes sure that the mock catalogs can cover the whole survey volume of the cluster catalog, the cell size of 5 h^{-1}Mpc is a half of the bin size of our correlation function measurements. The log-normal mock distribution is smooth at scales smaller than the cell size. Correlation functions are calculated for every mock catalog, the covariance matrix is then generated by:

$$C_{ij} = \frac{1}{N-1}\sum_{k=1}^{N}\left(\xi_i^k - \overline{\xi}_i\right)\left(\xi_j^k - \overline{\xi}_j\right), \quad (6)$$

where $N = 100$ is the number of mock catalogs, ξ_i^k is the correlation function value of the k^{th} mock at the i^{th} bin of r values, and $\overline{\xi}_i$ represents the mean value of the all 100 mock catalogs at the i^{th} bin. The error bars of $\xi(r)$ are given by the diagonal elements as $\sigma_i = \sqrt{C_{ii}}$.

The jackknife error estimation method is adopted for the mass weight comparison. The details about the jackknife method and the comparison between log-normal and jackknife covariance matrices are discussed in the appendix.

We calculate the correlation function and the uncertainty in 18 bins from 20 h^{-1}Mpc to 200 h^{-1}Mpc. The analysis are made not only on the whole sample of 79,091 clusters, but also on six sub-samples divided according to sky region (Northern Cap and Southern Cap), or the redshift ranges ($z \leq 0.35$ and $0.35 < z \leq 0.5$) or the different cluster mass ($M_{500} \leq 1 \times 10^{14} M_\odot$ and $M_{500} > 1 \times 10^{14} M_\odot$).

After that, we analyze the correlation function of galaxy clusters with a χ^2 fitting to a ΛCDM model. First, the linear matter power spectra $P_{\rm lin}(z, k)$ are computed at each central value of redshift bin shown in the Figure 2 using CAMB package (Lewis et al. 2000). The no-wiggle approximation of the linear matter power spectrum $P_{\rm nw}(z, k)$ is generated by fitting the matter power spectrum with the model described in Eisenstein & Hu (1998). The template power spectrum with non-linear evolution effects is (Xu et al. 2012)

$$P_{\rm template}(z, k) = (P_{\rm lin}(z, k) - P_{\rm nw}(z, k)) \exp\left(-\frac{k^2\Sigma_{\rm nl}^2}{2}\right) + P_{\rm nw}(z, k), \quad (7)$$

where $\Sigma_{\rm nl}$ is a parameter modeling the non-linear degradation (Eisenstein et al. 2007; Crocce & Scoccimarro 2008; Seo et al. 2008; Xu et al. 2012), we choose $\Sigma_{\rm nl} = 8$ h^{-1}Mpc in the analysis. The template correlation function with damped BAO at each redshift is then given by

$$\xi_{\rm template}(z, r) = \int \frac{k^2 dk}{2\pi^2} P_{\rm template}(z, k) j_0(kr) \exp\left(-k^2 a^2\right), \quad (8)$$

where $j_0(kr)$ is the zeroth-order spherical Bessel function, the Gaussian term gives a high-k damping during the transformation with $a = 1$ h^{-1}Mpc, which is significantly smaller than the scale of the structure we are interested in. The "averaged" template correlation function $\xi_{\rm template}(r)$ is then generated by weighting the template correlation functions at each redshift using the corresponding number counts $n(z)$ in the redshift bins. Finally, we fit the cluster correlation function using a model form of

$$\xi_{\rm model}(r) = b^2 \xi_{\rm template}(\alpha r) + A(r), \quad (9)$$

where

$$A(r) = \frac{a_1}{r^2} + \frac{a_2}{r} + a_3. \quad (10)$$

b^2, α, a_1, a_2 and a_3 are free parameters, b^2, a_1, a_2 and a_3 are marginalized finally. The χ^2 fitting runs in the parameter space of $0.80 \leq \alpha \leq 1.20$, where we fix the other cosmological parameters to the Planck 2015 values of $\Omega_b = 0.0484$, $n_s = 0.97$, $\sigma_8 = 0.81$, $\Omega_m = 0.31$, $\Omega_\Lambda = 0.69$ and $h = 0.68$. In this fiducial cosmology, the distance parameter D_v at redshift $z = 0.331$ is $D_v^{fid}(z = 0.331) = 1301.9$ Mpc.

3.1. *Results of the whole sample*

The correlation function of all 79,091 clusters is shown in Figure 4. We adopt a weight to correct the selec-

TABLE 1
BAO FITTING RESULTS OF THE CLUSTER SAMPLE AND SUB-SAMPLES

Sample	N	α	σ
Whole sample	79091	0.969 ± 0.037	3.7
North cap	57647	0.979 ± 0.058	2.2
South cap	21444	$\sim 0.939^{\star}$	0.7
$M_{500} > 1 \times 10^{14} M_{\odot}$	49207	0.979 ± 0.058	2.3
$M_{500} \leq 1 \times 10^{14} M_{\odot}$	29884	$0.960^{\star}$	0.6
$z \leq 0.35$	40873	0.938 ± 0.041	3.3
$0.35 < z \leq 0.50$	38218	1.020 ± 0.065	2.2

NOTE. — we cannot provide an effective error estimation for the α value for the 'Southern Cap' and 'low mass' sub-samples because of very weak signals.

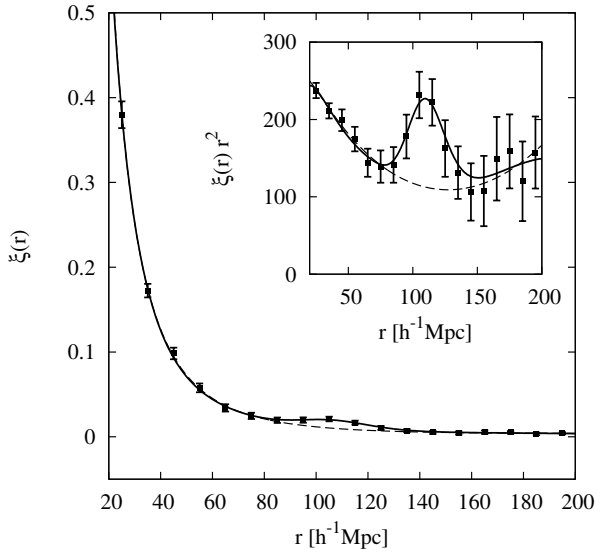

FIG. 4.— Correlation function of 79,091 clusters plotted by black squares with error bars. The solid line and dashed line indicate the best-fit ΛCDM model with and without acoustic feature. In the inset $\xi(r)r^2$ is plotted to show the BAO feature more clearly. The error bars are estimated via the log-normal method.

tion bias of the sample and cluster mass. The BAO feature appears at $r \sim 105\ h^{-1}$Mpc clearly. We do the χ^2 fitting using with the whole covariance matrix, and find the best-fit $\chi^2 = 6.77$ on 13 degrees of freedom, and the reduced $\chi^2 = 0.52$. A pure CDM model without the BAO feature is also adopted to fit the correlation function, which presents a $\chi^2 = 20.29$ and is rejected at 3.7σ. This is the first time of detecting the BAO signal from a galaxy cluster sample with a confidence larger than 3σ. The best-fit ΛCDM model offers a constraint on the parameter $\alpha = 0.969 \pm 0.037$, which gives a constraint on the distance parameter D_v by $D_v(z = 0.331) r_d^{fid}/r_d = 1261.5 \pm 48$ Mpc. See Table 1 for a summary.

We compare the correlation function of the whole cluster sample without weighting (i.e. all clusters share the same weight equals to 1), and compare the result in Figure 5. Since the log-normal method could not provide the cluster mass for the mock catalogs, so we use the jackknife method which employs the original cluster mass of the data catalog in this comparison. Because the net effect of the weighting algorithm is giving higher weights to more massive clusters, the weighting pulls the correlation function up to the higher amplitude with a detection confidence of 3.9σ, while the non-weighted calculation gives a confidence of 3.1σ. We conclude that the mass weight can help the BAO detection and dose not move the BAO signal position. The best fitted α value is $\alpha = 0.972$ with the mass weight, compared with $\alpha = 0.971$ without the mass weight. Therefore, the weightings are used in all following calculations for sub-samples.

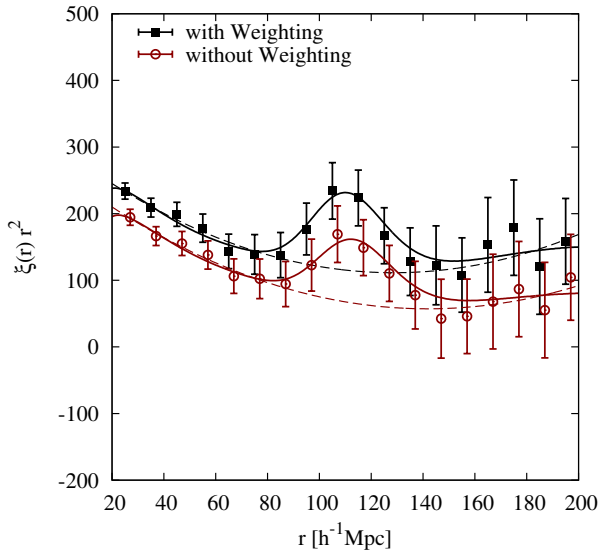

FIG. 5.— The correlation functions of the whole sample with (squares) and without (circles, shifted to right by 2 h^{-1}Mpc for clarity) weights during the calculations. The error bars are estimated by the jackknife method. The solid lines and dashed lines indicate the best-fit ΛCDM curves with and without acoustic feature.

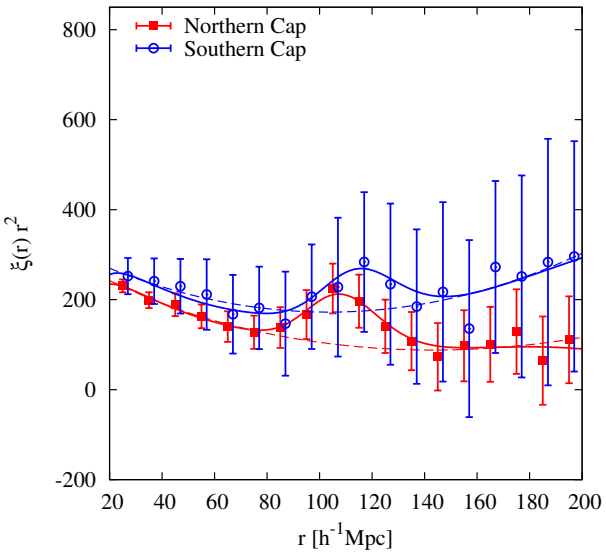

FIG. 6.— The correlation function for BAO detection from galaxy clusters in the Northern Cap (squares) and the Southern Cap (circles, shifted to right by 2 h^{-1}Mpc for clarity), as we do in Figure 4.

3.2. *Results for two sky regions*

We also calculate the correlation function with the weights for clusters in the Northern Cap and Southern Cap separately. The correlation functions are shown in the Figure 6 with the best-fit model lines. The BAO feature on the Northern Cap is clear, with a detection confidence of 2.2σ. Due to the smaller sample size, the

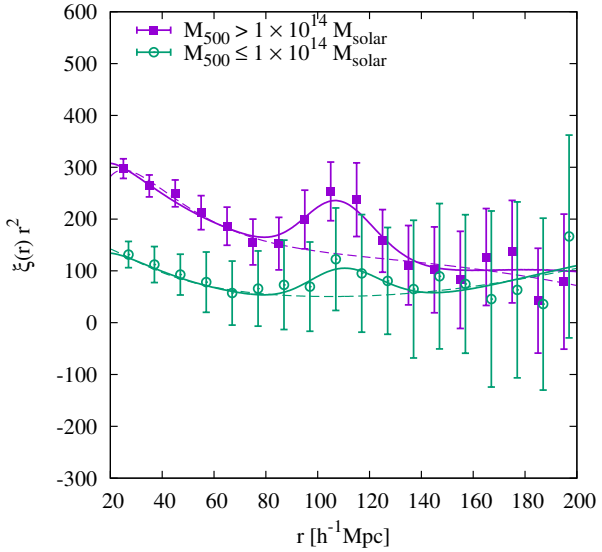

FIG. 7.— The same as Figure 6 but for the high mass sample (squares) and the low mass (circles, shifted to right by 2 h^{-1}Mpc for clarity) clusters.

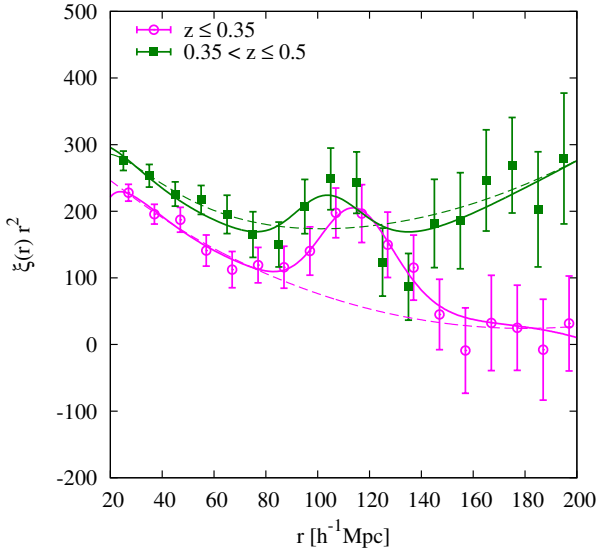

FIG. 8.— The same as Figure 6 but for clusters at high redshift (squares) and low redshift (circles, shifted to right by 2 h^{-1}Mpc for clarity).

BAO signal on the Southern Cap is week, which has a confidence of 0.7σ.

We notice that the correlation function of the Southern Cap sample has a higher amplitude comparing with the correlation function of the Northern Cap sample. The BAO bump on the correlation function of the Southern Cap sub-sample also shows a shift towards to the larger scale direction, the model fitting reports a central value of the distance parameter of $\alpha = 0.939$, which deviates from the model prediction, but the low signal-to-noise ratio of the BAO bump leads a difficulty to estimate the measuring accuracy, the flat χ^2 distribution makes the attempts of determining the 1σ error bar failed.

3.3. *Results for different mass ranges*

To compare the correlation function of clusters with different masses, we make two sub-samples. The high mass sub-sample contains 49,207 clusters with a mass of $M_{500} > 1 \times 10^{14} M_\odot$, the low mass sub-sample has 29,884 clusters with a mass of $M_{500} \leq 1 \times 10^{14} M_\odot$. The correlation functions of these two sub-samples are presented in the Figure 7. A clear BAO signal is detected in the high mass sub-sample with a confidence of 2.3σ, while the BAO bump of low mass sub-sample is very week, only 0.6σ. Like the 'Southern Cap' sub-sample, we cannot provide 1σ error for the low-mass sub-sample because of the low signal-to-noise ratio.

In small scales of $r < 80$ h^{-1}Mpc, we note the amplitude of correlation function for high mass clusters is systematically higher than the low mass ones. Hong et al. (2012) analyzed the correlation functions in small scales of sub-samples with different cluster richness, found that the correlation length and then the amplitude of the correlation function are proportional to the cluster richness. It is expected that clusters with high masses trace the more massive halos, which leads a stronger correlation than the low mass sub-sample. Therefore the result here is consistent with our previous conclusion.

3.4. *Results for different redshift ranges*

The whole sample is split into two sub-samples by the redshift. The low redshift sub-sample contains 40,873 clusters with the redshift of $z \leq 0.35$, the high redshift sub-sample contains 38,218 clusters in the redshift region of $0.35 < z \leq 0.5$. The correlation functions of high and low redshift sub-samples are shown in the Figure 8. Both of the correlation functions show BAO signals at the scale of $r \sim 105$ h^{-1}Mpc, the BAO peak detection confidence is 3.3σ and 2.2σ on the low and high redshift sub-samples, respectively.

The correlation amplitude is also found to be different for these two sub-samples with the scales of $r < 80$ h^{-1}Mpc. The difference is due to the different cluster mass distributions in the two samples. In the higher redshift region, luminous and massive galaxies have larger chances to be spectroscopically observed, which makes our high redshift sub-sample contains relatively more massive clusters than the low redshift sample. The mean mass of the high redshift sample is $M_{500} = 1.42 \times 10^{14} M_\odot$, while, the mean mass of the low redshift sample is $M_{500} = 1.24 \times 10^{14} M_\odot$.

3.5. *Discussions*

Tojeiro et al. (2014) calculated both the correlation function and power spectrum of 313,780 galaxies from SDSS DR11 over 7,341 square degrees, in the redshift range of $0.15 < z < 0.43$ with a mean redshift $\overline{z} = 0.32$. By fitting the BAO feature, they provided a distance measurement of $D_V(0.32) = 1264 \pm 25(r_d/r_{d,fid})$, with a measuring accuracy of 1.9%. In comparison, our cluster sample has a similar redshift coverage and contains 79,091 clusters, only about 25% of the galaxy sample size used by Tojeiro et al. (2014). We detect the BAO signal by 3.7σ and get a distance measurement of $D_v(z = 0.331) r_d^{fid}/r_d = 1261.5 \pm 48$ Mpc with a measuring accuracy of 3.8%. This implies a potential economical way to study the large-scale structures in the future. Spectroscopic observations are very time consuming especially for faint galaxies. When doing the large-scale structure studies using clusters, spectroscopic redshifts are not necessary for every galaxy. We can identify galaxy clusters

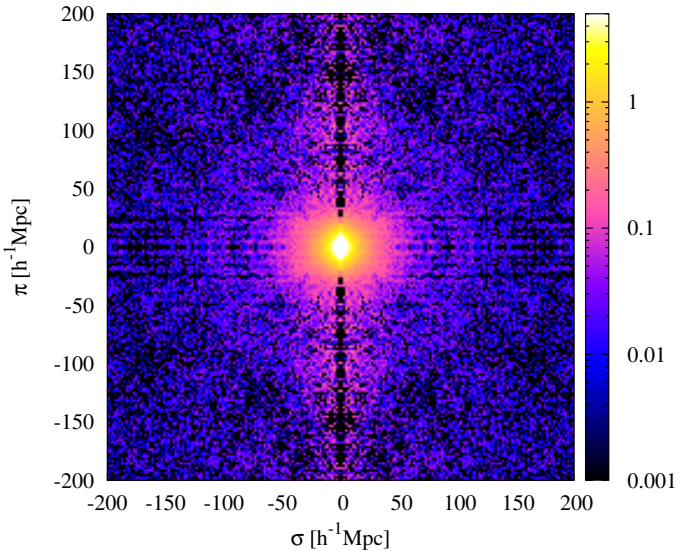

FIG. 9.— The 2D correlation function of the 79,901 clusters. The correlation function is binned in 2 h^{-1}Mpc bins.

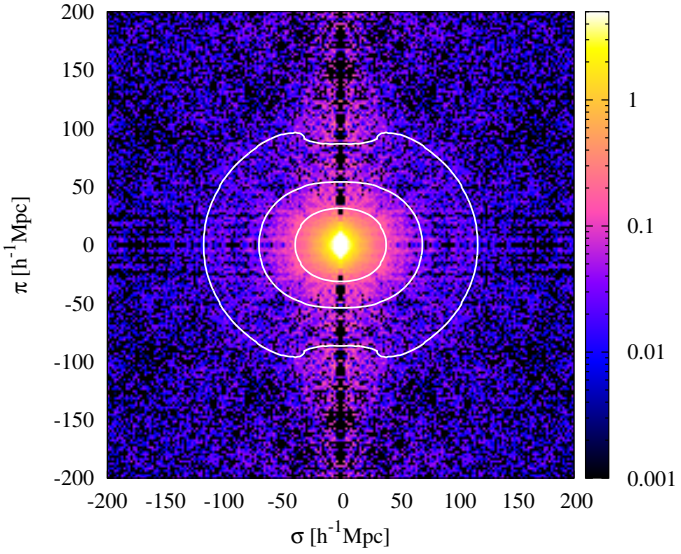

FIG. 10.— 2D correlation function with the best-fit theoretical correlation function as white contours.

from photometry survey data first, and does the spectroscopic follow-up for BCGs which are bright and can be easily observed. A much smaller sample of clusters can provide a fairly accurate measurement to the cosmological parameters too. We noticed that after this paper was submitted, Veropalumbo et al. (2016) calculated the 2-point correlation function using the cluster catalog presented by Wen et al. (2012) and got a distance measurement consistent with ours.

4. THE 2D CORRELATION FUNCTION

We calculate the 2D correlation function of the 79,901 clusters following the same estimator and same weighting method described by Equation 2 and Equation 4. The result is shown in Figure 9, where π is the separation between two clusters along the line-of-sight and σ is the separation across the line-of-sight. The faint BAO ring appears at the scale of $r \sim 105\ h^{-1}$Mpc.

Following Hamilton (1992) and Chuang & Wang (2013) we build a theoretical 2D correlation function:

$$\xi_{\rm template}(\sigma,\pi) = \xi_0^{\rm template}(r)P_0(\mu) + \xi_2^{\rm template}(r)P_2(\mu) + \xi_4^{\rm template}(r)P_4(\mu), \quad (11)$$

with

$$\xi_0^{\rm template}(r) = \left(1 + \frac{2\beta}{3} + \frac{\beta^2}{5}\right)\xi(r), \quad (12)$$

$$\xi_2^{\rm template}(r) = \left(\frac{4\beta}{3} + \frac{4\beta^2}{7}\right)[\xi(r) - \overline{\xi}(r)], \quad (13)$$

$$\xi_4^{\rm template}(r) = \frac{8\beta^2}{35}\left[\xi(r) + \frac{5}{2}\overline{\xi}(r) - \frac{7}{2}\overline{\overline{\xi}}(r)\right], \quad (14)$$

where $r = \sqrt{\sigma^2+\pi^2}$, μ is the cosine of the angle between the direction of cluster and the LOS, $\beta = \Omega_m^{0.55}/b$. $P_0(\mu) = 1$, $P_2(\mu) = \frac{1}{2}\left(3\mu^2-1\right)$ and $P_4(\mu) = \frac{1}{8}\left(35\mu^4 - 30\mu^2 + 3\right)$ are the Legendre polynomials and

$$\overline{\xi}(r) = \frac{3}{r^3}\int_0^r \xi(r')r'^2 dr', \quad (15)$$

$$\overline{\overline{\xi}}(r) = \frac{5}{r^5}\int_0^r \xi(r')r'^4 dr', \quad (16)$$

where $\xi(r)$ is the theoretical correlation function generated from the matter power spectrum provided by the CAMB package using the same cosmological parameters adopted by the theoretical two-point correlation function. Finally, the model correlation function is given by:

$$\xi_{\rm model}(\sigma,\pi) = b^2\xi_{\rm template}(\alpha_\sigma\sigma, \alpha_\pi\pi) + \frac{a_1}{r^2} + \frac{a_2}{r} + a_3, \quad (17)$$

where $\alpha_\sigma, \alpha_\pi, a_1, a_2, a_3$ and the bias b are free parameters, a_1, a_2, a_3 and b are marginalized.

By fitting this model to the result in Figure 9, we neglect the component of 'Finger-of-God' (Jackson 1972) which arises at the small scales (e.g. Peacock et al. 2001; Ross et al. 2007; Beutler et al. 2012), and focus on the feature of BAO ring at the scale range of 40 h^{-1}Mpc $\leq r \leq$ 150 h^{-1}Mpc in the parameter space of $0.80 \leq \alpha_\sigma \leq 1.20$ and $0.80 \leq \alpha_\pi \leq 1.20$. We find the best-fit scale parameters of $\alpha_\sigma = 1.02 \pm 0.06$ and $\alpha_\pi = 0.94 \pm 0.10$, respectively. By replacing the theoretical correlation function $\xi(r)$ with a no-wiggle correlation function $\xi^{nw}(r)$ in the Equations 12 to 16, we build a no-wiggle 2D correlation function model, and find the difference of the fitting χ^2 between the models with and without baryon feature is $\Delta\chi^2 = 3.4$ which provides a BAO ring detection confidence of 1.8σ. The best-fit model correlation function is plotted as contours with the cluster correlation function in Figure 10.

5. CONCLUSIONS

We build a galaxy cluster sample based on the updated cluster catalog published by Wen & Han (2015), which contains 79,901 clusters in the redshift range of $z \leq 0.5$ with a mean redshift $\overline{z} = 0.331$. All these clusters have spectroscopic redshift measurements from the SDSS DR12 data (Alam et al. 2015).

We calculate the 2-point correlation function of the cluster sample with a weight of cluster mass and sample

completeness. The weighting algorithm not only corrects the selection bias introduced by the cluster identifying process but also enhances the BAO signal on the final correlation function. A baryon acoustic peak is detected at the scale of $r \sim 105\ h^{-1}$Mpc, with a detection confidence of 3.7σ. This is the first time to detect a significant BAO signal using a galaxy cluster sample. By fitting the observed correlation function using a ΛCDM model, we find a constraint of $\alpha = 0.969 \pm 0.037$ and $D_v(z = 0.331)r_d^{fid}/r_d = 1261.5 \pm 48$ Mpc, which show a great consistency with the fiducial cosmology obtained by the Planck 2015 data.

We also calculate the 2D correlation function of the cluster sample. The faint BAO ring emerges at the scale of $r \sim 105\ h^{-1}$Mpc. By fitting the correlation function using a theoretical 2D correlation function, we detect the BAO ring with a detection confidence of 1.8σ. Though it is not good enough to detect the BAO feature in the separated two directions, we get the constraint on the distance parameters of $\alpha_\sigma = 1.02 \pm 0.06$ and $\alpha_\pi = 0.94 \pm 0.10$.

We conclude that the BAO detection via spectroscopically observed BCGs can easy the survey job, because one can find galaxy clusters first via photometric data, and then do spectroscopic observations for a much smaller sample of galaxies.

We thank X. Y. Gao, G. B. Zhao, Y. T. Wang and F. Beutler for useful discussions and comments. The authors are supported by the National Natural Science Foundation of China (11473034). TH and ZLW are also supported by the Young Researcher Grant of National Astronomical Observatories, Chinese Academy of Sciences.

APPENDIX

A COMPARISON OF COVARIANCE MATRICES ESTIMATED BY THE LOG-NORMAL AND JACKKNIFE METHODS

The jackknife method estimates the covariance matrix by making sub-samples based on the original data catalog (internal estimate), which is somehow different from the external estimate based on N-body simulations or the log-normal realizations. By comparing the covariance matrix estimated of the internal and external methods on the scales of $0.1 - 40\ h^{-1}$Mpc, Norberg et al. (2009) found the jackknife method overestimates the variance on small scales of $\lesssim 2 - 3\ h^{-1}$Mpc, but it works fine on larger scales of $\gtrsim 10\ h^{-1}$Mpc. On the BAO scales of $\sim 100\ h^{-1}$Mpc, Beutler et al. (2011) concluded that the jackknife error is noisier and larger than the log-normal error for the 6dFGS galaxy sample. Here we compare the covariance matrices of the correlation function estimated by the log-normal and jackknife methods.

We obtain the jackknife covariance matrix by dividing the sky area into 32 disjoint sub-regions, each sub-region has approximately the same area with others. The jackknife method is found to be robust when changing the number of jackknife sub-samples (Veropalumbo et al. 2016). The 32 jackknife sub-samples are built by removing the clusters in one sub-region, ensuring that each sub-region is removed in one sub-sample only. The correlation function is calculated for each sub-sample following Equation 2. The covariance matrix is then built up as:

$$C_{ij} = \frac{N-1}{N} \sum_{k=1}^{N} \left(\xi_i^k - \overline{\xi}_i\right)\left(\xi_j^k - \overline{\xi}_j\right), \qquad \text{(A1)}$$

where $N = 32$ is the number of sub-samples, ξ_i^k is the correlation function value of the k^{th} sub-sample at the i^{th} bin of r values, and $\overline{\xi}_i$ represents the mean value of the all 32 sub-samples at the i^{th} bin.

We show the jackknife error in Figure 11 together with the log-normal error as a comparison. The jackknife error is found to be larger than the log-normal error in most of the bins, it is also noisier than the log-normal error. Besides the diagonal term of the covariance matrix, we

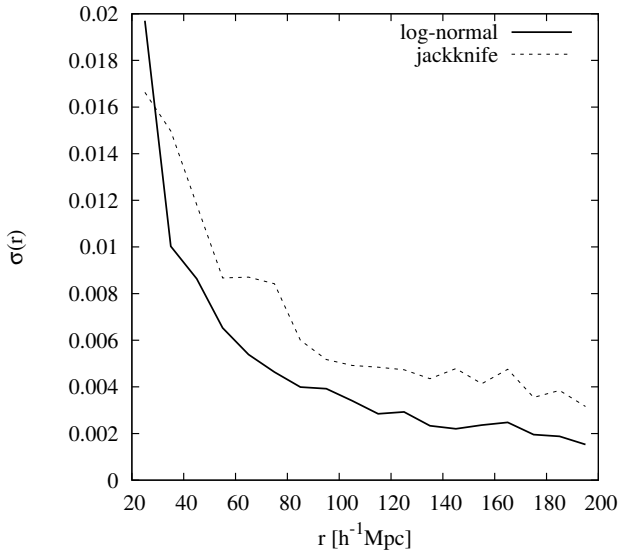

FIG. 11.— The correlation function errors estimated by the log-normal method (solid line) and the jackknife method (dashed line) respectively.

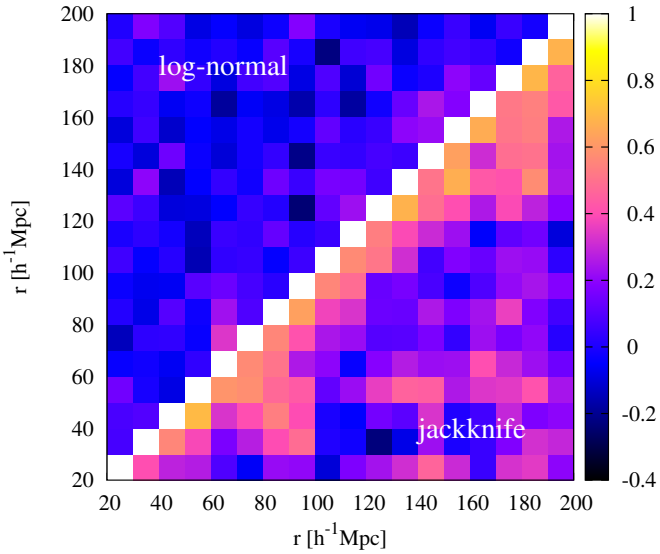

FIG. 12.— The correlation matrix of the log-normal errors and jackknife errors.

also show the full matrix in Figure 12. The covariance estimated by the log-normal method is much smoother than the one estimated by the jackknife method. The elements plotted in Figure 12 are defined as:

$$r_{ij} = \frac{C_{ij}}{\sqrt{C_{ii}C_{jj}}}, \tag{A2}$$

where C is the covariance matrix.

We noticed that Veropalumbo et al. (2016) also compared the covariance matrices of the jackknife method and the log-normal method using a galaxy cluster sample with SDSS III spectroscopic redshift, and they found a similar conclusion as ours.

REFERENCES

Alam, S., Albareti, F. D., Allende Prieto, C., et al. 2015, ApJS, 219, 12
Anderson, L., Aubourg, E., Bailey, S., et al. 2012, MNRAS, 427, 3435
—. 2014, MNRAS, 439, 83
Beutler, F., Blake, C., Colless, M., et al. 2011, MNRAS, 416, 3017
—. 2012, MNRAS, 423, 3430
Blake, C., & Bridle, S. 2005, MNRAS, 363, 1329
Blake, C., Davis, T., Poole, G. B., et al. 2011, MNRAS, 415, 2892
Busca, N. G., Delubac, T., Rich, J., et al. 2013, A&A, 552, A96
Chuang, C.-H., & Wang, Y. 2013, MNRAS, 435, 255
Cole, S., Percival, W. J., Peacock, J. A., et al. 2005, MNRAS, 362, 505
Coles, P., & Jones, B. 1991, MNRAS, 248, 1
Colless, M., Dalton, G., Maddox, S., et al. 2001, MNRAS, 328, 1039
Crocce, M., & Scoccimarro, R. 2008, Phys. Rev. D, 77, 023533
Delubac, T., Bautista, J. E., Busca, N. G., et al. 2015, A&A, 574, A59
Eisenstein, D. J., & Hu, W. 1998, ApJ, 496, 605
Eisenstein, D. J., Seo, H.-J., & White, M. 2007, ApJ, 664, 660
Eisenstein, D. J., Zehavi, I., Hogg, D. W., et al. 2005, ApJ, 633, 560
Estrada, J., Sefusatti, E., & Frieman, J. A. 2009, ApJ, 692, 265
Geller, M. J., & Huchra, J. P. 1989, Science, 246, 897
Gott, III, J. R., Jurić, M., Schlegel, D., et al. 2005, ApJ, 624, 463
Hamilton, A. J. S. 1992, ApJ, 385, L5
Hong, T., Han, J. L., Wen, Z. L., Sun, L., & Zhan, H. 2012, ApJ, 749, 81
Hütsi, G. 2010, MNRAS, 401, 2477
Jackson, J. C. 1972, MNRAS, 156, 1P
Kazin, E. A., Blanton, M. R., Scoccimarro, R., et al. 2010, ApJ, 710, 1444
Koester, B. P., McKay, T. A., Annis, J., et al. 2007a, ApJ, 660, 239
—. 2007b, ApJ, 660, 221
Landy, S. D., & Szalay, A. S. 1993, ApJ, 412, 64
Lewis, A., Challinor, A., & Lasenby, A. 2000, ApJ, 538, 473
Norberg, P., Baugh, C. M., Gaztañaga, E., & Croton, D. J. 2009, MNRAS, 396, 19
Peacock, J. A., Cole, S., Norberg, P., et al. 2001, Nature, 410, 169
Peebles, P. J. E., & Yu, J. T. 1970, ApJ, 162, 815
Percival, W. J., Cole, S., Eisenstein, D. J., et al. 2007, MNRAS, 381, 1053
Planck Collaboration, Ade, P. A. R., Aghanim, N., et al. 2015, ArXiv e-prints, arXiv:1502.01589
Ross, N. P., da Ângela, J., Shanks, T., et al. 2007, MNRAS, 381, 573
Scrimgeour, M. I., Davis, T., Blake, C., et al. 2012, MNRAS, 425, 116
Seo, H.-J., Siegel, E. R., Eisenstein, D. J., & White, M. 2008, ApJ, 686, 13
Sunyaev, R. A., & Zeldovich, Y. B. 1970, Ap&SS, 7, 3
Tegmark, M., Eisenstein, D. J., Strauss, M. A., et al. 2006, Phys. Rev. D, 74, 123507
Tojeiro, R., Ross, A. J., Burden, A., et al. 2014, MNRAS, 440, 2222
Veropalumbo, A., Marulli, F., Moscardini, L., Moresco, M., & Cimatti, A. 2014, MNRAS, 442, 3275
—. 2016, MNRAS, 458, 1909
Wen, Z. L., & Han, J. L. 2015, ApJ, 807, 178
Wen, Z. L., Han, J. L., & Liu, F. S. 2009, ApJS, 183, 197
—. 2012, ApJS, 199, 34
Xu, X., Padmanabhan, N., Eisenstein, D. J., Mehta, K. T., & Cuesta, A. J. 2012, MNRAS, 427, 2146
York, D. G., Adelman, J., Anderson, Jr., J. E., et al. 2000, AJ, 120, 1579
Zhan, H., Wang, L., Pinto, P., & Tyson, J. A. 2008, ApJ, 675, L1